**Spacer length matters**: The influence of the length of polyyne spacers on the optoelectronic properties of push–pull chromophores was comprehensively investigated in a combined experimental and theoretical study. The high solubility of chromophores allowed for INADEQUATE NMR measurements without $^{13}C$ labeling, thus providing unique insight into the π-electron delocalization along the polyyne chain. Very high, off-resonant specific third-order optical nonlinearities were measured at a spacer length of two and three triple bonds.

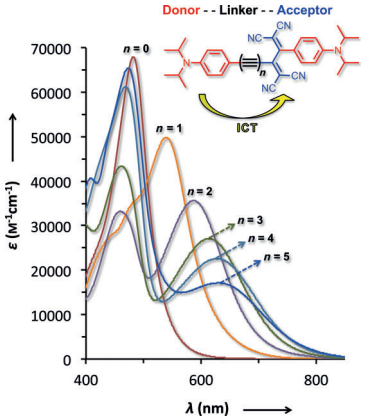


Donor–Acceptor Chromophores

*M. Štefko, M. D. Tzirakis, B. Breiten, M.-O. Ebert,* O. Dumele, W. B. Schweizer, J.-P. Gisselbrecht, C. Boudon, M. T. Beels, I. Biaggio,* F. Diederich** ..... ▮▮▮▮–▮▮▮▮

**Donor–Acceptor (D–A)-Substituted Polyyne Chromophores: Modulation of Their Optoelectronic Properties by Varying the Length of the Acetylene Spacer**

CHEMISTRY
A EUROPEAN JOURNAL

ChemPubSoc
Europe

DOI: 10.1002/chem.201301642

# Donor–Acceptor (D–A)-Substituted Polyyne Chromophores: Modulation of Their Optoelectronic Properties by Varying the Length of the Acetylene Spacer

**Martin Štefko,[a] Manolis D. Tzirakis,[a] Benjamin Breiten,[a] Marc-Olivier Ebert,*[a] Oliver Dumele,[a] W. Bernd Schweizer,[a] Jean-Paul Gisselbrecht,[b] Corinne Boudon,[b] Marten T. Beels,[c] Ivan Biaggio,*[c] and François Diederich*[a]**

*Dedicated to Professor Martin Quack on the occasion of his 65th birthday*

**Abstract:** A series of donor–acceptor-substituted alkynes, **2a**–**f**, was synthesized in which the length of the π-conjugated polyyne spacer between the *N*,*N*-diisopropylanilino donor and the 1,1,4,4-tetracyanobuta-1,3-diene (TCBD) acceptor was systematically changed. The effect of this structural change on the optoelectronic properties of the molecules and, ultimately, their third-order optical nonlinearity was comprehensively investigated. The branched *N*,*N*-diisopropyl groups on the anilino donor moieties combined with the nonplanar geometry of **2a**–**f** imparted exceptionally high solubility to these chromophores. This important property allowed for performing INADEQUATE NMR measurements without $^{13}C$ labeling, which, in turn, resulted in a complete assignment of the carbon skeleton in chromophores **2a**–**f** and the determination of the $^{13}C$–$^{13}C$ coupling constants. This body of data provided unprecedented insight into characteristic $^{13}C$ chemical shift patterns in push–pull-substituted polyynes. Electrochemical and UV/Vis spectroscopic studies showed that the HOMO–LUMO energy gap decreases with increasing length of the polyyne spacer, while this effect levels off for spacers with more than four acetylene units. The third-order optical nonlinearity of this series of molecules was determined by measuring the rotational averages of the third-order polarizabilities ($\gamma_{rot}$) by degenerate four-wave mixing (DFWM). These latter studies revealed high third-order optical nonlinearities for the new chromophores; most importantly, they provided fundamental insight into the effect of the conjugated spacer length in D–A polyynes, that can be exploited in the future design of suitable charge-transfer chromophores for applications in optoelectronic devices.

**Keywords:** charge-transfer · INADEQUATE · nonlinear optics · polyynes · push–pull chromophores

## Introduction

Donor–acceptor (D–A) chromophores continue to attract considerable interest due to their electronic and optical properties, and particularly their second- and third-order optical nonlinearities.[1] Most of the known D-π-A chromophores feature a planar molecular scaffold to ensure efficient π-conjugation between the donor and the acceptor moieties.[2–10] These planar chromophores tend to form crystalline films by virtue of strong π–π stacking interactions and antiparallel molecular dipole alignment in the solid state.[11] Their employment in optoelectronic devices, however, requires the formation of amorphous thin films which can achieve high homogeneity and optical quality over large areas.[12] Thus, the design of suitable nonplanar chromophores[13] that avoid the formation of crystalline films, is of upmost importance for their practical applications.

Since the mid-1990s, we reported high third-order optical nonlinearities for five classes of small push–pull chromophores: donor–acceptor-substituted tetraethynylethenes (TEEs),[8] donor-substituted cyanoethynylethenes (CEEs),[9,10] donor-substituted 1,1,4,4-tetracyanobuta-1,3-dienes (TCBDs),[14,15]

[a] Dr. M. Štefko, Dr. M. D. Tzirakis, Dr. B. Breiten, Dr. M.-O. Ebert, O. Dumele, Dr. W. B. Schweizer, Prof. Dr. F. Diederich
Laboratorium für Organische Chemie, ETH Zürich
Hönggerberg, HCI, 8093 Zurich (Switzerland)
Fax: (+41) 44-632-1109
Fax: (+41) 44-632-1475
E-mail: ebert@org.chem.ethz.ch
diederich@org.chem.ethz.ch

[b] Dr. J.-P. Gisselbrecht, Prof. Dr. C. Boudon
Laboratoire d'Electrochimie et de Chimie Physique du Corps Solide, Institute de Chimie-UMR 7177, CNRS
Université de Strasbourg, 4, rue Blaise Pascal
CS 90032, 67081 Strasbourg Cedex (France)

[c] M. T. Beels, Prof. Dr. I. Biaggio
Lehigh University, Department of Physics
415 Lewis Lab, 16 Memorial Dr. East, Bethlehem, PA 18015 (USA)
Fax: (+1) 610-758-5730
E-mail: biaggio@lehigh.edu

Supporting information for this article is available on the WWW under http://dx.doi.org/10.1002/chem.201301642.

  

homoconjugated push–pull systems,[16] and more recently *N,N′*-dicyanoquinone diimide-derived D–A chromophores.[17] Especially in one of these studies we showed that a nonplanar *N,N*-dimethylanilino (DMA)-substituted TCBD, namely 2-[4-(dimethylamino)phenyl]-3-{[4(dimethylamino)phenyl]ethynyl}buta-1,3-diene-1,1,4,4-tetracarbonitrile; DDMEBT (**1**)) exhibits a large third-order nonlinear optical response despite its small number of delocalized π-electrons (Figure 1 a).[14] Most importantly, it is this

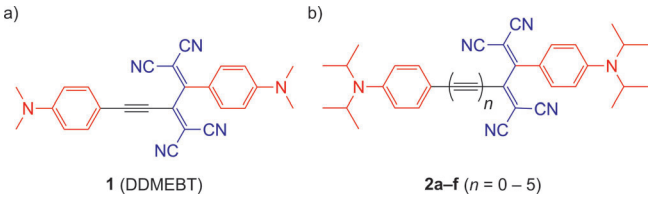


Figure 1. a) Structure of the DDMEBT chromophore (**1**) employed in previous studies and device fabrication.[14,18,19] b) D–A chromophores **2a–f** with polyyne spacers of different length investigated in this project.

very nonplanar geometry of DDMEBT that allows it to form dense, high-optical quality homogeneous films upon vapor deposition; these films have been elaborated into nonlinear optical silicon-organic hybrid slot waveguides for all-optical high-speed signal processing with excellent performance.[18,19]

The use of polyyne spacers in D–A conjugates and, in particular, the intramolecular charge-transfer (CT) and the nonlinear optical (NLO) properties of such systems have long been studied on both a theoretical and experimental basis.[20–28] Typically, the off-resonant, that is, nonabsorptive, third-order polarizability strongly increases as the energy associated with the transition from the ground to the first excited state (HOMO–LUMO gap) decreases.[29] More specific investigations on the third-order NLO properties of polyynes without D–A substitution have shown that their molecular second hyperpolarizabilities ($\gamma$) increase as a function of the number of acetylene units ($n$) according to the power-law $\gamma \approx n^{4.28\pm0.13}$.[30–32] Similarly, in D–A-substituted polyynes, polarizability depends on the length of the linear D–A conjugation pathways.[33,34] Thus, stronger D–A coupling across shorter π-conjugated spacers leads to hypsochromic shifts, whereas weaker D–A coupling across longer spacers results in smaller HOMO–LUMO gaps and hence bathochromically shifted CT bands.[35,36] In D–A chromophores of given spacer size, the HOMO–LUMO gap decreases with increasing π-conjugation efficiency.[37]

The role of the acetylenic groups as spacers in push–pull chromophores has been comprehensively studied for donor-substituted cyanoethynylethenes (CEEs).[9,38,39] The introduction of alkynyl spacers ($n$ = 0–3) in these chromophores resulted in less readily homogeneous solutions due to the resulting planar molecular geometry and concomitant low solubility.[39] Also, there were indications that saturation of the third-order polarizability could already be reached at the diyne stage, but the weak solubility did not allow a full characterization.[39] On the other hand, a donor-substituted TCBD with a five-triple-bond spacer displayed good solubility and showed a very strong third-order optical nonlinearity for self-phase modulation at a wavelength 1.5 μm, which suggested a high potential for NLO applications of alkyne spacers in suitably designed chromophores.[40]

In this work, we present a systematic study on the influence of the acetylene spacer length in TCBD-derived push–pull chromophores. To this end, we have prepared a series of push–pull chromophores **2a–f**, in which the number of the acetylene bonds in the polyyne spacer between the anilino donor and the TCBD acceptor varies systematically from 0 to 5 (Figure 1 b).

The presence of the branched *N,N*-diisopropylamino moieties combined with the nonplanar geometry of **2a–f** enhances the solubility of these chromophores, thus allowing for performing NMR (INADEQUATE) and NLO measurements in common organic solvents such as $CH_2Cl_2$ ($CD_2Cl_2$) or $CHCl_3$ ($CDCl_3$). Furthermore, it should be noted that the TCBD unit exhibits enhanced electron-accepting ability with respect to the dicyanovinyl moiety used in the planar, donor-substituted CEEs.[7]

## Results and Discussion

**Synthesis of oligoynes 3a–f and D–A chromophores 2a–f**: All TCBD chromophores **2a–f** were prepared in moderate to excellent isolated yields (50–92 %) by the thermal [2+2] cycloaddition–retroelectrocyclization (CA–RE) reaction[41] between the corresponding *N,N*-diisopropylanilino-end-capped oligoynes **3a–f** and tetracyanoethylene (TCNE) in $CH_2Cl_2$ at 25 °C (Scheme 1).

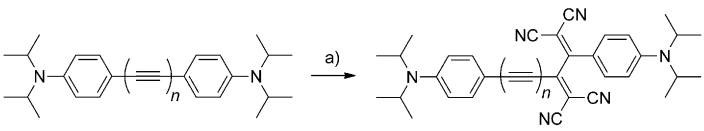


**3a** (*n* = 1) **3d** (*n* = 4)
**3b** (*n* = 2) **3e** (*n* = 5)
**3c** (*n* = 3) **3f** (*n* = 6)

**2a** (*n* = 0, 90%) **2d** (*n* = 3, 60%)
**2b** (*n* = 1, 92%) **2e** (*n* = 4, 56%)
**2c** (*n* = 2, 83%) **2f** (*n* = 5, 50%)

Scheme 1. Synthesis of D–A chromophores **2a–f** by the CA-RE reaction of oligoynes **3a–f** with TCNE. a) TCNE, $CH_2Cl_2$, 25 °C, 6 h. TCNE = tetracyanoethylene.

The synthesis of oligoynes **3a–f** started from 4-ethynyl-*N,N*-diisopropylaniline (**4**) prepared on a multigram scale by a conceptually new protocol (see Scheme 1SI in the Supporting Information). Monoyne **3a** was prepared by Sonogashira cross-coupling reaction of 4-bromo-*N,N*-diisopropylaniline with terminal acetylene **4** in 58 % yield (see Scheme 2SI in the Supporting Information). Diyne **3b** and tetrayne **3d** were obtained by following well-established synthetic protocols[42,43] by an oxidative homocoupling reaction of the corresponding terminal mono- and di-acetylenes in 88 % and 45 % overall yield, respectively, based on **4** (see Scheme 3SI and 5SI in the Supporting Information). Triyne

**3c** was prepared from **4** in 28% yield over 4 steps; the last critical step included a Fritsch–Buttenberg–Wiechell (FBW) rearrangement[44–47] of the corresponding symmetrical *gem*-dibromoolefin[48] (see Scheme 4SI in the Supporting Information). The synthesis of pentayne **3e** started from terminal acetylene **4** which, after treatment with *n*BuLi at −18°C, was allowed to react with triisopropylsilylpropargyl aldehyde[49] to give pentadiynol **5** in 90% yield (Scheme 2). Subsequently, the oxidation of alcohol **5** by $BaMnO_4$ provided,

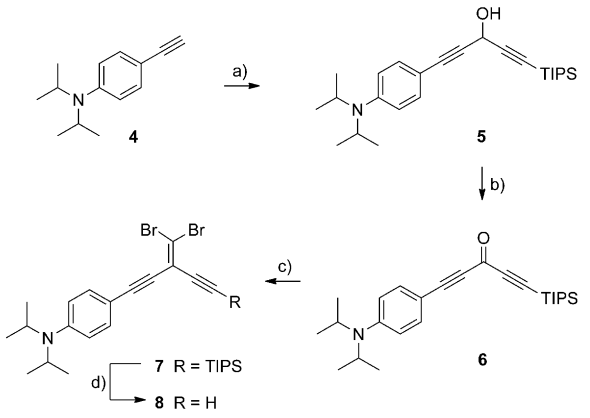


Scheme 2. Synthesis of intermediate **8**: a) *n*BuLi, $Et_2O$, −78°C, 20 min, then TIPS−C≡C−CHO, −78°C, 30 min, 90%; b) $BaMnO_4$, $CH_2Cl_2$, 25°C, 30 min, 98%; c) $P(OiPr)_3$, $CBr_4$, $CH_2Cl_2$, 0°C, 1.5 h, 83%; d) TBAF, THF, 0°C, 20 min, 96%. TIPS = triisopropylsilyl; TBAF = tetra-*n*-butylammonium fluoride; THF = tetrahydrofuran.

after a simple filtration of manganese salts, pure ketone **6** in quantitative yield (Scheme 2). The Horner–Wadsworth–Emmons modification of the Ramirez *gem*-dibromoolefination[50] was then used to transform ketone **6** into *gem*-dibromoolefin **7**. Thus, a solution of ketone **6** was treated at 0°C with $CBr_4$ in the presence of $P(OiPr)_3$ furnishing **7** as a bench-stable orange oil in 83% yield (Scheme 2). Cleavage of the TIPS-protecting group was accomplished upon treatment with $nBu_4NF$ giving terminal acetylene **8** in 96% yield.

Lithium acetylide, generated from **8** upon treatment with LDA in $Et_2O$ at −78°C, was subsequently allowed to react with aldehyde **9** to give alcohol **10** in 84% yield,[32] which was further oxidized by $BaMnO_4$ furnishing ketone **11** in quantitative yield (Scheme 3). Aldehyde **9** was prepared in 76% yield by the reaction of lithium acetylide (generated form **4** upon treatment with *n*BuLi at −18°C) with DMF (Scheme 3). Subsequent *gem*-dibromoolefination of **11** furnished bis(*gem*-dibromoolefin) **12** in 75% yield (Scheme 3). In the final step, a two-fold FBW rearrangement of **12** gave pentayne **3e** in 46% yield (Scheme 3). Stable crystals, suitable for X-ray analysis, were obtained by slow diffusion of hexanes into a solution of **3e** in $CH_2Cl_2$ at 25°C (Scheme 3; see also Figure 3SI in the Supporting Information).

The final member of this series of chromophores, hexayne **3f**, was prepared in 50% yield over two steps by oxidative homocoupling of terminal acetylene **8** and subsequent two-fold FBW rearrangement of the resulting bis-dibromoolefin (see Scheme 6SI in the Supporting Information).

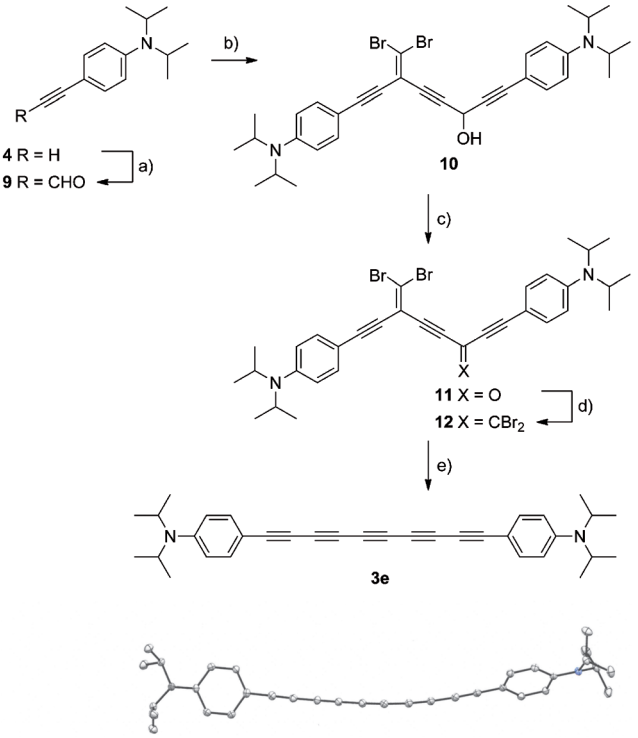


Scheme 3. Synthesis and ORTEP plot of pentayne **3e**: a) *n*BuLi, −18°C, THF, 10 min, then DMF, −18°C, 30 min, 76%; b) **8**, LDA, −78°C, $Et_2O$, 30 min, then **9**, −78°C, 30 min, 84%; c) $BaMnO_4$, $CH_2Cl_2$, 25°C, 1 h, 98%; d) $P(OiPr)_3$, $CBr_4$, $CH_2Cl_2$, 0°C, 1 h, 75%; e) *n*BuLi, toluene, −78°C to −10°C, 30 min, 46%. THF = tetrahydrofuran; DMF = dimethylformamide; LDA = Lithium diisopropylamide. A second independent molecule in the unit cell of **3e** is shown in Figure 3SI in the Supporting Information.

**$^{13}$C NMR chemical shifts and assignments**: Due to the lack of protons in large parts of chromophores **2a–f**, the $^{13}$C chemical shift assignment by HSQC/HMBC is not possible. Assignments of longer polyynes available in the literature have been achieved so far by specific $^{13}$C labeling.[32] The excellent solubility of chromophores **2a–f** in $CDCl_3$, which results from the presence of the branched *N,N*-diisopropylamino moieties and is further enhanced by the nonplanar geometry of the push–pull systems, allowed us to prepare NMR samples concentrated enough for chemical shift assignment by INADEQUATE spectroscopy, without $^{13}$C labeling.[51–53] All assigned spectra are shown in Figure 2. A summary of the chemical shifts for the carbon atoms in the acetylenic linkers of chromophores **2b–f** is provided in Table 1 (for the list of all carbons, see Table 1SI in the Supporting Information). Alongside the resonances of C3′ and C18′ carbons in the aniline rings, the other two carbon signals at lowest field belong to C7′ and C9′ of the TCBD moiety. The resonances of the neighboring C8′ and C10′ carbons in α-position relative to the cyano groups are shifted to higher field by more than 50 ppm. This pattern is characteristic for the shifts of $sp^2$ carbons adjacent to a dicyanomethylene group (e.g., in benzylidene malononitrile)[54] and can be rationalized by a favorable resonance structure bearing the positive charge at

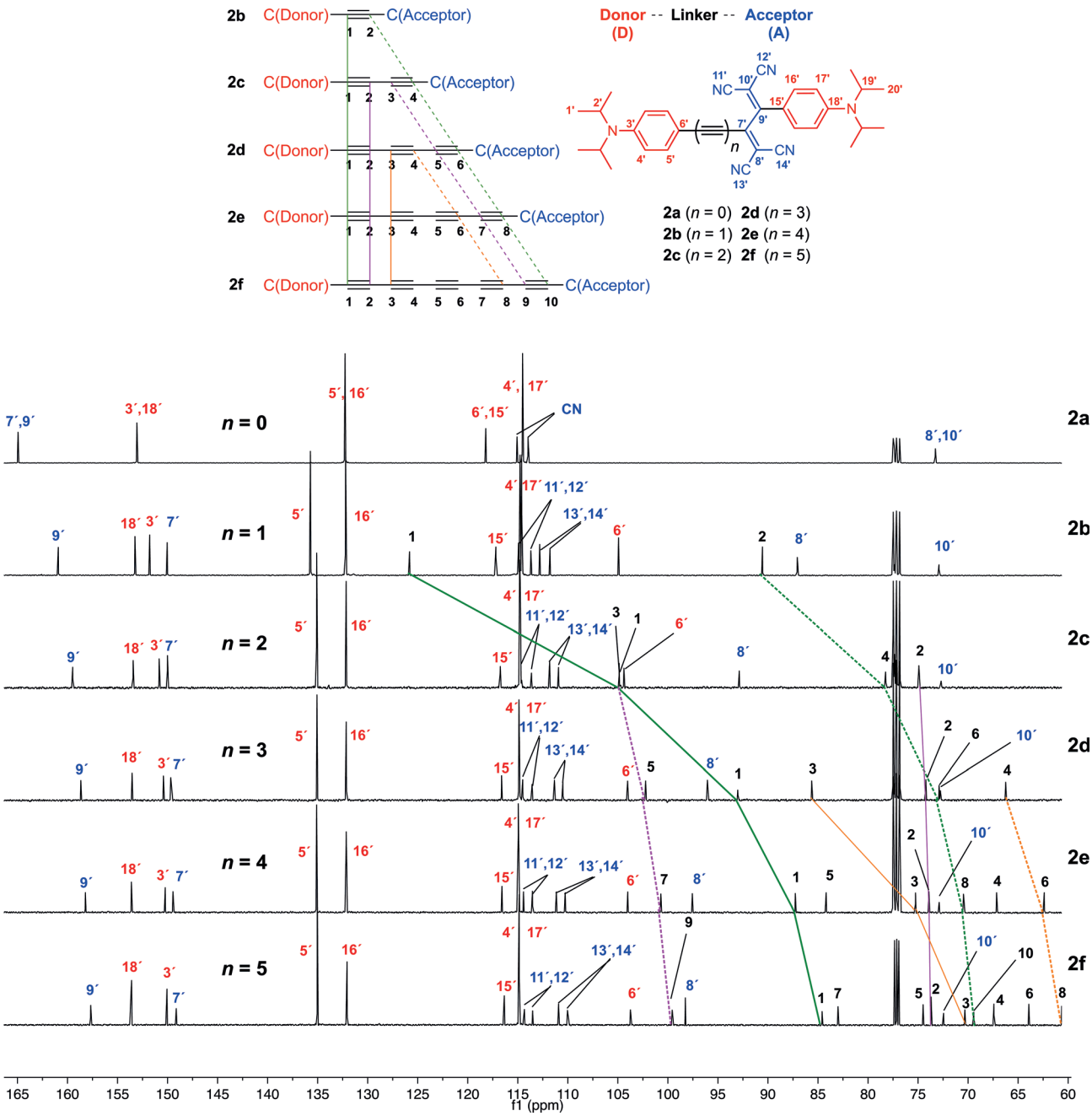


Figure 2. Assignment of the $^{13}$C NMR resonances for chromophores **2a–f**. Parts of the spectrum below 60 ppm are omitted for clarity. The colored lines connect the acetylenic carbons with the same distances from the aniline donor (D) or the TCBD acceptor (A). The following changes in chemical shift as a function of increasing polyyne length are specifically highlighted: i) resonances of C1 directly attached to the donor (green line), ii) C-atoms in α-position to the acceptor (dotted green line), iii) C2 atoms next to the donor (magenta line), iv) C-atoms in β-position to the acceptor (dotted magenta line), v) C3 atoms next to the donor (orange line), and iv) C-atoms in γ-position to the acceptor (dotted orange line).

the β-carbon, whereas the negative charge is positioned at one of the cyano groups. In the series **2a–f**, there is a rather large difference in chemical shift between carbons at position 8′ (more than 20 ppm), whereas the $^{13}$C shifts at position 10′ are unaffected by the length of the polyyne linker (see Figure 4SI in the Supporting Information). This finding can be accounted for by the existence of two independent intramolecular CT pathways: one pathway involves CT from the distant aniline to the dicyanovinyl acceptor via the acetylene spacer, whereas the other pathway involves a CT from the second diisopropylanilino donor directly to the adjacent dicyanovinyl acceptor. This latter pathway, which involves the dicyano group at C10′ and the adjacent aniline, is decoupled from the polyyne and therefore not markedly affected by the length of the linker (vide infra).

Figure 2 also highlights the change in the chemical shift of the polyyne carbons with the same distance from the anilino donor or the TCBD acceptor, respectively, as a function of

Table 1. Summary of the chemical shifts ($\delta$, ppm) for the acetylenic carbons in chromophores **2b–f**.[a]

| | | Chemical shifts ($\delta$, ppm)[a] | | | | | | | | | |
|---|---|---|---|---|---|---|---|---|---|---|---|
| | $n$[b] | C1 | C2 | C3 | C4 | C5 | C6 | C7 | C8 | C9 | C10 |
| **2b** | 1 | 125.81 | 90.55 | – | – | – | – | – | – | – | – |
| **2c** | 2 | 104.78[c] | 74.92[c] | 104.86 | 78.25 | – | – | – | – | – | – |
| **2d** | 3 | 93.02 | 74.22 | 85.63 | 66.24 | 102.23 | 72.9 | – | – | – | – |
| **2e** | 4 | 87.27 | 73.91 | 75.25 | 67.15 | 84.18 | 62.39 | 100.7 | 70.46 | – | – |
| **2f** | 5 | 84.62 | 73.77 | 70.28 | 67.47 | 74.57 | 63.96 | 83.03 | 60.66 | 99.60 | 69.44 |

[a] Chemical shifts are given in ppm and are referenced to the signal of $CDCl_3$ (77.16 ppm). [b] $n$ = number of C≡C units in the spacer between the anilino donor and the TCBD acceptor. [c] The assignment of C1 and C2 was achieved by combination of INADEQUATE and HMBC (400 MHz) measurements (cross-peak between H5′ and C1).

chain length. With growing chain, the resonances at each position are gradually shifted to higher field, with the odd-numbered C-atom resonances (C-atoms 1, 3) with respect to the donor affected more than the even-numbered ones (C-atoms 2) (solid lines, Figure 2). Similarly, the resonances of carbons at odd distance to the acceptor shift more than those at even distance (dashed lines, Figure 2). These individual trends, which are in agreement with those reported by Tykwinski and Luu for symmetrically substituted derivatives,[55] may be explained with the inductive effect of the polyyne chain. The same authors have also reported a steady decrease in chemical shift of the carbon atoms in the center of the chain with growing chain length together with a polarization of the chemical shifts at the level of the individual carbon chains, that is, chemical shifts at even and odd positions are grouped together.[55] An analogous plot for **2a–f** is shown in Figure 3a. Because of the asymmetric substitution of the polyyne chain, here two individual decaying curves are obtained. The curves suggest a convergence of the chemical shifts of the central atoms of this type of donor–acceptor system in a region around 70 ppm. If we only plot the chemical shifts of the polyyne linker of **2f** without the terminal atoms 1 and 10 (Figure 3b), the increase of the chemical shifts at the odd positions with increasing distance to the donor, together with a significant, albeit less pronounced decrease of the chemical shifts at the even positions with increasing distance to the donor, leads to two individually decaying curves connecting even and odd carbon resonances, respectively. The intersection of the curves leads to a breakdown of a strict alternation for **2f** (still intact in **2e**) and will obscure it further for longer chains. For donor–acceptor systems, such as **2a–f**, the alternating chemical shifts may be rationalized by a series of resonance structures that all locate the positive charge on carbons 1, 3, 5, 7, 9 with odd distances to the donor group and the negative charge on carbons 2, 4, 6, 8, 10 with even positions from the donor group. Together, this result would suggest an alternating partial charge separation leading to deshielded odd carbons and shielded even carbons, thus explaining the downfield shift of the odd versus the even positions. Indeed, the Hirshfeld atomic charges[56] of **2d** calculated in Gaussian 09[57] at the B3LYP/6-311+G(d,p) level of theory are weakly positive for the odd and negative for the even positions (values: 0.002, −0.05, 0.006, −0.02, 0.003, −0.03 for C1 to C6 of the polyyne linker, respectively).

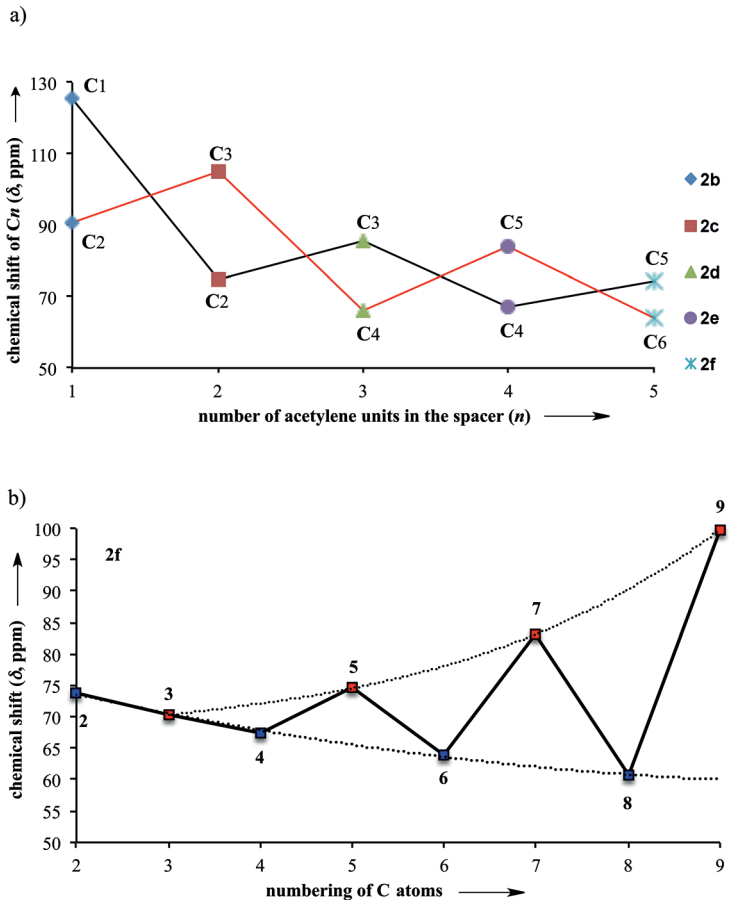


Figure 3. a) Chemical shift ($\delta$, ppm) of the C-atoms at the chain center plotted versus chain length. The black line connects the shifts of the central acetylenic C-atoms on the side of the anilino donor. The red line connects the shifts of the central acetylenic C-atoms on the side of the dicyanovinyl acceptor. b) Chemical shifts ($\delta$, ppm) of the C-atoms in chromophore **2f**. C-atom numbering according to Figure 2.

In agreement with this explanation, for the $^{13}C$ shifts of two di-*tert*-butyl-end-capped polyynes reported by Bohlmann and Brehm ($C_{16}H_{18}$ and $C_{18}H_{18}$)[58] where neither donor nor acceptor is present, no alternation in chemical shift but only a decay towards the central carbon atoms was observed. This simple argument, however, does not explain the sense of polarization observed for α,ω-diphenylpolyynes.[55] Here, one would expect the π-donor effect of the two phenyl groups (at least close to the polyyne termini) to lead to higher shielding of the even positions compared to the odd ones. Conversely, Tykwinski and Luu have found that for these molecules the odd positions are shifted towards higher field.[55] Clearly, a better understanding of the influence of the electronic structure on the $^{13}C$ chemical shifts is still needed.

Table 2. Summary of the $^1J(^{13}C–^{13}C)$ coupling constants in the acetylenic spacer of chromophores **2b–f**.[a]

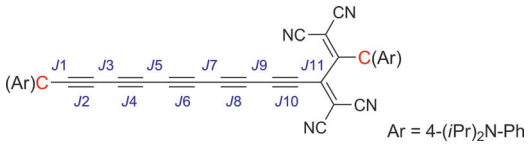


| | | Coupling constants[a] | | | | | | | | | | |
|---|---|---|---|---|---|---|---|---|---|---|---|---|
| | $n$[b] | $J1$ | $J2$ | $J3$ | $J4$ | $J5$ | $J6$ | $J7$ | $J8$ | $J9$ | $J10$ | $J11$ |
| **2b** | 1 | 95 | 187 | 100 | – | – | – | – | – | – | – | – |
| **2c** | 2 | –[c] | 194 | –[c] | 202 | 101 | – | – | – | – | – | – |
| **2d** | 3 | 94 | 198 | 162 | 215 | 167 | 205 | 99 | – | – | – | – |
| **2e** | 4 | 94 | 195 | 166 | 213 | 172 | 215 | 168 | 206 | 101 | – | – |
| **2f** | 5 | 95 | 195 | –[c] | –[c] | 170 | 215 | 171 | 217 | 169 | 205 | 102 |

[a] Coupling constants are given in Hz. [b] $n$ = number of C≡C units in the spacer between the anilino donor and the TCBD acceptor. [c] Not determined.

**$^{13}C–^{13}C$ coupling constants**: Inspection of the cross-peak fine structure in the INADEQUATE spectra of **2a–f** allowed for a straightforward extraction of $^1J(^{13}C–^{13}C)$ coupling constants (for **2e**, see Figure 4; for all compounds of the series, see Figure 5SI in the Supporting Information). Outside the polyyne spacer, the coupling constants are nearly constant throughout the series **2a–f**. In contrast to the chemical shifts, there is also very little variation among coupling constants between spacer atoms at the same relative position (Table 2). The coupling constants corresponding to the two outermost triple bonds are close to 200 Hz with the one between the two carbons directly adjacent to the TCBD moiety being the larger one of the two by approximately 10 Hz. The coupling constants corresponding to the inner triple-bonds are around 215 Hz. The ones corresponding to the formal $C_{sp}–C_{sp}$ single bonds are between 160 and 170 Hz. The only exception is **2b** with a coupling constant of only 187 Hz between the carbon atoms forming the triple bond.

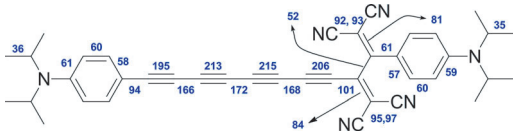


Figure 4. $^1J(^{13}C–^{13}C)$ coupling constants; chromophore **2e** is shown as a representative example (complete data for the whole series **2a–f** are shown in Figure 5SI in the Supporting Information).

**UV/Vis spectroscopy**: Figure 5 depicts the UV/Vis absorption spectra of CT chromophores **2a–f** recorded in $CH_2Cl_2$ at 25 °C. A detailed discussion of the UV/Vis spectra of the oligoyne precursors **3a–f** is provided in the Supporting Information. All chromophores **2a–f** feature a broad, low-energy transition that is assigned to the intramolecular charge-transfer (ICT) transition resulting from excitation from the anilino donor at the polyyne termini to the TCBD acceptor. The CT nature of this band was confirmed by treating a solution of these chromophores in $CH_2Cl_2$ with $CF_3COOH$, leading to attenuation of the CT band; the band re-appeared when the acidified solution was treated with $NEt_3$ (see Figure 9SI in the Supporting Information). The energy of this CT band decreases with increasing spacer length; for example, the longest-wavelength maximum ($\lambda_{max}$)

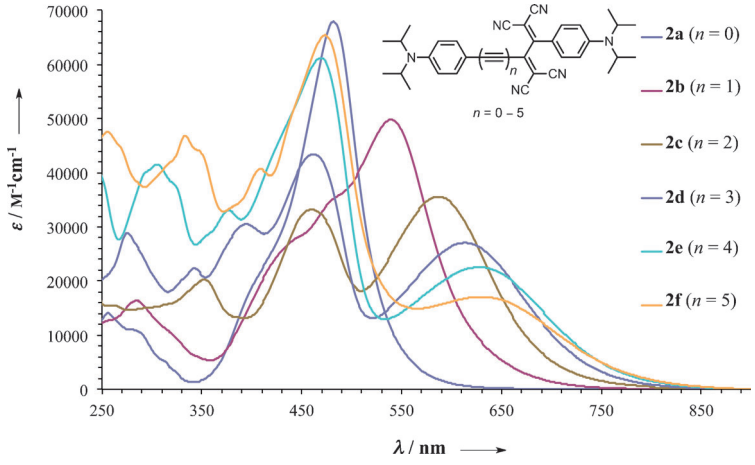


Figure 5. UV/Vis spectra ($CH_2Cl_2$, 25 °C) of chromophores **2a–f** with different number of C≡C units in the spacer between the diisopropylanilino donor and the TCBD acceptor.

increases from 482 nm (2.57 eV) for **2a** ($n=0$) to 629 nm (1.97 eV) for **2f** ($n=5$) (Table 3). More specifically, the D–A chromophore **2a** ($n=0$) displays an intense CT band at 482 nm with molar absorption coefficient $\varepsilon(\lambda_{max})=$ 66800 $M^{-1}cm^{-1}$ (Table 3, entry 1), whereas the corresponding CT band of chromophore **2b** ($n=1$) is bathochromically shifted by 57 nm with concomitant decrease in absorption [$\varepsilon(\lambda_{max})=49200\,M^{-1}cm^{-1}$] (Table 3, entry 2). Starting from **2c** ($n=2$) the absorption spectrum is split into two separated CT bands, including, in particular, one high-energy band with $\lambda_{1,max}=460$ nm (2.70 eV, 31800 $M^{-1}cm^{-1}$) and one low-energy band with $\lambda_{max}=586$ nm (2.12 eV, 36200 $M^{-1}cm^{-1}$) (Table 3, entry 3). With increasing acetylenic spacer length, the low-energy band in **2d** ($n=3$) is bathochromically shifted to $\lambda_{max}=613$ nm (2.02 eV) accompanied by a decrease in intensity (28000 $M^{-1}cm^{-1}$). On the other hand, the high-energy band is bathochromically shifted by only 2 nm to $\lambda_{1,max}=462$ nm (2.68 eV) accompanied—in contrast to the low-energy band—by an increase in intensity from $\varepsilon(\lambda_{1,max})=31800\,M^{-1}cm^{-1}$ (**2c**) to 44900 $M^{-1}cm^{-1}$ (**2d**). The same trend continues for the rest of the series (Table 3, Figure 5; see also Figure 22SI in the Supporting Information). The $\lambda_{max}$ values in this series of chromophores level off at 628 nm (1.97 eV) for **2e** ($n=4$) and **2f** ($n=5$), thus suggesting a saturation of the D–A interactions. Furthermore, chromophores **2c** ($n=2$) and **2d** ($n=3$) display positive solvatochromism; the change of solvent from *n*-hexane to $CH_2Cl_2$ resulted in a bathocromic shift of the longer-wavelength CT band by 56 and 59 nm for **2c** and **2d**, respectively (see Figures 23SI–24SI in the Supporting Information).

Table 3. UV/Vis data ($CH_2Cl_2$, 25 °C) for chromophores **2a–f** with different number of C≡C units in the spacer between the anilino donor and the TCBD acceptor.

| Entry | Compd | $n$[a] | $\lambda_{1,max}$[b] [nm (eV)] | $\varepsilon(\lambda_{1,max})$ [$M^{-1}cm^{-1}$] | $\lambda_{max}$ [nm (eV)] | $\varepsilon(\lambda_{max})$ [$M^{-1}cm^{-1}$] |
|---|---|---|---|---|---|---|
| 1 | **2a** | 0 | – | – | 482 (2.57) | 66800 |
| 2 | **2b** | 1 | – | – | 539 (2.30) | 49200 |
| 3 | **2c** | 2 | 460 (2.70) | 31800 | 586 (2.12) | 36200 |
| 4 | **2d** | 3 | 462 (2.68) | 44900 | 613 (2.02) | 28000 |
| 5 | **2e** | 4 | 469 (2.64) | 60300 | 628 (1.97) | 22300 |
| 6 | **2f** | 5 | 473 (2.62) | 68800 | 629 (1.97) | 17900 |

[a] $n$ = number of C≡C units in the acetylene spacer. [b] $\lambda_1$ values for compounds **2c–f** refer to the high-energy transition.

The slight differences observed for the $\lambda_{1,max}$ values of **2c–f** compared to the large bathochromic shift of the $\lambda_{max}$ values (see Figure 22SI in the Information), can be ascribed to the different influence of the spacer length on the two CT pathways. Thus, an increase in the spacer length influences only the ICT from the distant anilino donor via the spacer to the adjacent dicyanovinyl group; this results in a remarkable bathochromic shift of the ICT absorption ($\lambda_{max}$) by 147 nm upon moving from **2a** to **2f**. On the other hand, the CT from the anilino donor to the directly connected dicyanovinyl group ($\lambda_{1,max}$) displays only a slight bathochromic shift (from 460 nm in **2c** to 473 nm in **2f**). This observation confirms that this latter CT is almost independent on the spacer length, and that both CT interactions are essentially independent from each other. Similar conclusions have been drawn on the basis of the NMR investigations presented above.

Finally, the UV/Vis spectra of **2a–f** show that the CT band at the longest wavelength ($\lambda_{max}$) is broader than the one at lower wavelength ($\lambda_{1,max}$) and broadens with increasing the spacer length. This effect should be ascribed to the flexibility of the acetylene spacer in solution, which increases with increasing length and results in a larger variety of low-frequency molecular vibrational modes in the longer acetylene linkers.

To further support the above-mentioned findings, we prepared the corresponding series of *N,N*-dimethylamino analogues **13a** ($n=0$), **1** ($n=1$), and **13c,d** ($n=2$, 3) (Figure 6) and their UV/Vis spectra were directly compared to those of **2a–d** ($n=0$–3) (see Figure 20SI and 21SI; see also Figure 16SI–19SI in the Supporting Information). These measurements supported fully the aforementioned conclusions regarding the effect of the spacer length on the optoelectronic properties of (D–A)-substituted acetylene chromophores. A further comparison between the UV/Vis spectra of these two series of chromophores revealed a small bathochromic shift of all ICT bands of **2a–d** with respect to those of **13a**, **1** and **13c,d**, accompanied by a small increase in intensity (see Figure 21SI in the Supporting Information). This effect should be ascribed to the stronger electron-donating ability of the *N,N*-diisopropylanilino donor as compared to its dimethylanilino analogue.[43]

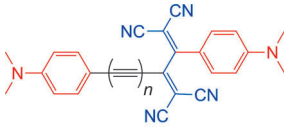


**13a** ($n=0$)
**1** ($n=1$)
**13c** ($n=2$)
**13d** ($n=3$)

Figure 6. *N,N*-Dimethylanilino-derived chromophores **13a**,[14] **1**,[14] **13c**, and **13d**.[42]

**Computational studies**: The vertical optical transitions of the optimized molecular structures of **2a–f** were calculated by time-dependent density functional theory (TD-DFT; for further details on the computational methods, see the Supporting Information). In all cases, the computed transition energies are slightly larger than the experimental values (see Table 4SI–9SI in the Supporting Information). Differences between computed excitation energies and experimental absorption maxima are in the range of 0.15–0.37 eV (mean absolute deviation of 0.27 eV), well within the expected error.[59–61] The comparison of the computed and the experi-

mental absorption in the low-energy transitions shows a similar trend (see Figure 25SI in the Supporting Information); with increasing spacer length, the absorption maxima show bathochromic shifts reaching a plateau starting with the tetrayne spacer. The plateau energy is due to the centering of HOMO and LUMO on the donor and acceptor, which is a characteristic of these (D–A)-substituted polyynes. Without D–A substitution, the $\lambda_{max}$ values would be expected to keep growing for longer spacers as it was observed for the corresponding non-(D–A)-substituted polyynes **3a–f** (see Figure 8SI in the Supporting Information).[62] Also without D–A substitution, the absolute value of $\lambda_{max}$ would have been much smaller (see Figure 8SI in the Supporting Information).[30]

The lowest-energy transitions are composed mostly of HOMO-to-LUMO excitations and thus can best be described as intramolecular charge-transfer processes involving the transfer of electron density from the anilino donor to the dicyanovinyl acceptor in compound **2a** ($n=0$) and from the distant anilino donor via the acetylene linker to the adjacent dicyanovinyl acceptor moiety in compounds **2b–f** ($n=1$–5) as depicted in the molecular orbital representations of these levels (see Table 4SI–9SI in the Supporting Information). Interestingly, with increasing length of the acetylene spacer all orbitals involved in the discussed excitations become less diffuse and get clearly separated, reaching almost no overlap in the electron density on the donor and acceptor moieties for the case of the pentayne spacer (**2f**), although a certain overlap of the HOMO and LUMO density on the acetylenic spacer is still observed (Figure 7). This effect is also reflected in the decrease of the transition dipole moment ($M$) (see the Supporting Information, Section 6.3), the decrease of the extinction coefficient ($\varepsilon$) of the low-energy absorptions ($\lambda_{max}$), and the decrease of the off-resonant third-order polarizability for the longer-spacer chromophores **2e**,**f** (vide infra). Further detailed discussion of the frontier orbitals of **2a–f** and the resulting effect on the transition dipole moments ($M$) is given in the Supporting Information (Section 6.3).

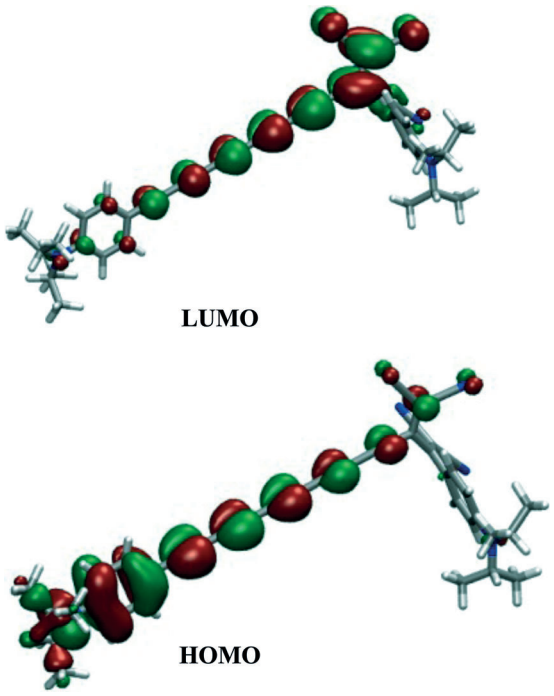


Figure 7. The HOMO (bottom) and LUMO (top) orbitals of **2f**. Further information for the other orbitals involved in **2f**, as well as for **2a–e**, is given in the Supporting Information.

The higher-energy transitions (at 460–473 nm) mainly consist of CT from HOMO−1-to-LUMO (for **2a–c**) and HOMO−1-to-LUMO+1 (**2d–f**). This computational finding suggests that this CT results from the transition from the anilino donor adjacent to the TCBD acceptor; the orbital pictures confirm this trend to a certain extent. The HOMO−1 electron density is mainly on the anilino moiety adjacent to the TCBD moiety and transfers to the conjugated dicyano group. However, from the diyne to the pentayne spacer in **2c–f**, a significant electron density on the acetylenic units is observed for the LUMO+1 orbital (which is, however, only significantly involved in that high-energy transition in the case of **2d–f**). This behavior clearly shows the electronic communication between the two twisted intramolecular donor–acceptor parts and shows the influence of the acetylenic spacer on the neighboring D–A system; this influence explains particularly the small bathochromic shift of the higher-energy excitations (460–473 nm) with increasing spacer length.

**Electrochemistry**: Electrochemical investigations were carried out by cyclic voltammetry (CV) (see Figure 27SI in the Supporting Information) and rotating disk voltammetry (RDV) in $CH_2Cl_2$ containing 0.1 M $n$Bu$_4$NPF$_6$ on a glassy carbon electrode (Table 4). All potentials are given versus $Fc^+/Fc$ (ferrocenium/ferrocene couple), which was used as an internal reference.

All chromophores **2a–f** gave rise to two reversible one-electron reductions located on the TCBD moiety. Only in the case of pentayne **2f**, a third irreversible reduction was observed. The reduction potentials are anodically shifted as a function of increasing number of acetylenic units between the donor and the acceptor. Thus, the first two reversible one-electron reductions are shifted from −1.15 and −1.31 V for **2a** to −0.59 and −0.94 V for **2f** (Table 4; see also Figure 28SI in the Supporting Information), respectively, as a result of the spacer extension.

The first oxidation, located on the anilino unit separated from the TCBD acceptor by the alkynyl spacer, is facilitated with increasing spacer length. Thus, the aniline ring transfers less electron density into the acceptor moiety which results in a dramatic cathodic shift of the first oxidation potential from 0.81 V in **2a** to 0.56 V in **2f** (Table 4; see also Figure 29SI in the Supporting Information). On the other hand, the second oxidation of the aniline ring adjacent to the TCBD moiety did not differ much throughout the whole series (0.92 V in **2a** to 0.89 V in **2f**, Table 4; see also Figure 29SI in the Supporting Information). This is in agree-

Table 4. Electrochemical data observed by cyclic voltammetry (CV; scan rate $\nu = 0.1$ $Vs^{-1}$) and rotating disk voltammetry (RDV) in $CH_2Cl_2$ (+ 0.1 M $nBu_4NPF_6$).[a]

| | CV | | | RDV | |
|---|---|---|---|---|---|
| | $E°$ [V][b] | $\Delta E_p$ [mV][c] | $E_p$ [V][d] | $E_{1/2}$ [V][e] | slope [mV][f] |
| **2a** | +0.92 | 60 | | +0.95 (1e$^-$) | 60 |
| | +0.81 | 60 | | +0.84 (1e$^-$) | 60 |
| | −1.15 | 110 | | −1.19 (1e$^-$) | 90 |
| | −1.31 | 100 | | −1.36 (1e$^-$) | 80 |
| **2b** | +0.90 | 80 | | +0.93 (1e$^-$) | 60 |
| | +0.69 | 80 | | +0.71 (1e$^-$) | 60 |
| | −0.91 | 110 | | −0.92 (1e$^-$) | 80 |
| | −1.16 | 100 | | −1.19 (1e$^-$) | 80 |
| **2c** | +0.90 | 100 | | +0.90(1e$^-$) | 70 |
| | +0.64 | 60 | | +0.62 (1e$^-$) | 70 |
| | −0.76 | 100 | | −0.78 (1e$^-$) | 70 |
| | −1.07 | 100 | | −1.11 (1e$^-$) | 90 |
| **2d** | +0.91 | 80 | | +0.91 (1e$^-$) | 70 |
| | +0.59 | 70 | | +0.62 (1e$^-$) | 70 |
| | −0.67 | 110 | | −0.71 (1e$^-$) | 110 |
| | −1.05 | 120 | | −1.07 (1e$^-$) | 120 |
| **2e** | +0.90 | 90 | | +0.91 (1e$^-$) | 70 |
| | +0.57 | 75 | | +0.58 (1e$^-$) | 70 |
| | −0.62 | 100 | | −0.65 (1e$^-$) | 70 |
| | −0.97 | 100 | | −1.04 (1e$^-$) | 80 |
| **2f** | +0.89 | 80 | | +0.85 | [g] |
| | +0.56 | 60 | | +0.53 (1e$^-$) | 75 |
| | −0.59 | 60 | | −0.58 (1e$^-$) | 60 |
| | −0.94 | 60 | | −0.95 (1e$^-$) | 60 |
| | | | −2.15 | −2.05 (1e$^-$) | 110 |

[a] All potentials are given versus $Fc^+$/Fc, which was used as internal standard. [b] $E° = (E_{pc} + E_{pa})/2$, where $E_{pc}$ and $E_{pa}$ correspond to the cathodic and anodic peak potentials, respectively. [c] $\Delta E_p = E_{pa} - E_{pc}$. [d] $E_p$ = irreversible peak potential. [e] $E_{1/2}$ = half-wave potential. [f] Slope = slope of the linearized plot of $E$ versus $\log[I/(I_{lim} - I)]$, where $I_{lim}$ is the limiting current and $I$ the current. [g] Electrode inhibition.

ment with the small wavelength shift observed by UV/Vis spectroscopy for the CT from the anilino donor directly connected to the dicyanovinyl acceptor group.

**Nonlinear optical properties**: The rotational average of the third-order polarizability $\gamma_{rot}$ of **2a–f** was determined by measuring the third-order susceptibility $\chi^{(3)}{}_{1111}(-\omega, -\omega, \omega, \omega)$ of $CH_2Cl_2$ solutions of varying molecular concentration. The measurements were taken by degenerate four-wave mixing (DFWM) at 1.5 μm using 1 ps laser pulses obtained from a TOPAS travelling wave optical parametric amplifier system pumped by a Clark MXR Ti:Sapphire amplifier. We used 1 mm thick solutions in fused silica spectroscopy cells, the concentrations of which were varied by successive dilutions and determined for each solution from the absorption spectrum calibrated to the spectrum of the molecular extinction coefficient, accurately measured by using solutions with varying molecular concentration (Figure 5; see also Figure 10SI–19SI in the Supporting Information). In addition, the higher concentration cells were calibrated by comparing the absorption spectrum in the semi-transparent spectral region between cells with neighboring concentrations. This guarantees an accurate determination of the molecular concentration responsible for the four-wave mixing signal even in those cases in which it was not possible to accurately control solvent evaporation and solute molecular mass for each dilution step. In addition, comparison of the absorption spectrum of the weakest concentration solution with the reference spectrum before and after the DFWM experiments confirmed the absence of any decomposition or contamination during the measurements.

For low concentrations, the third-order susceptibility of the solution depends on the concentration $C$ in units of mass of the solute divided by mass of the solution as $\chi^{(3)}{}_{1111}(C) = \chi^{(3)}{}_{1111}(0) + C f^4 \gamma_{rot} \rho/m$, where $f = (n^2+2)/3$ is a Lorentz local field factor that depends on the refractive index $n = 1.42$ of $CH_2Cl_2$, $\rho$ is the mass density of $CH_2Cl_2$, and $m$ is the mass of the molecule under investigation. The DFWM measurement determines the absolute value squared of $\chi^{(3)}{}_{1111}(C)$ for different values of $C$. We obtained absolute values for $\gamma_{rot}$ by a reference measurement that established the value of $\chi^{(3)}{}_{1111}(C{=}0)$ (for a cell filled with pure $CH_2Cl_2$) to be $6 \pm 1$ times larger than for a 1 mm thick fused silica sample, and using a third-order susceptibility of $\chi^{(3)}{}_{1111}(-\omega, -\omega, \omega, \omega) = 1.9 \times 10^{-22}$ for fused silica at 1.5 μm.

Table 5 lists the results for the third-order polarizability of molecules **2a–f**, as well as **13a**, **1**, and **13c**,**d**. In Table 5 we also list one more quantity that is useful for judging the nonlinear optical properties of a molecule, namely the specific third-order polarizability ($\gamma_S$), obtained by dividing the experimental value for the third-order polarizability $\gamma_{rot}$ by the molecular mass;[10] this quantity determines the potential bulk third-order susceptibility of a dense supramolecular assembly of molecules.

The nonlinear response of each molecule measured at 1.5 μm increases strongly with each addition of a triple bond in the spacer. The extended TCBD **2f** exhibits a large, reso-

Table 5. Summary of the NLO relevant characteristics ($CH_2Cl_2$, 25 °C) of the molecules investigated in this study.[a]

| Compound | $N_\pi$ | $n$ | $\lambda_{max}$ [nm] | $\varepsilon(\lambda_{max})$ [$10^3$ $M^{-1}cm^{-1}$] | $\gamma_{rot}$ [$10^{-48}$ $m^5V^{-2}$] | $\gamma_S$ [$10^{-23}$ $m^5V^{-2}Kg^{-1}$] |
|---|---|---|---|---|---|---|
| **2a** | 24 | 0 | 482 | 66.8 | 2±1 | 0.24 |
| **2b** | 26 | 1 | 539 | 49.2 | 6±2 | 0.68 |
| **2c** | 28 | 2 | 586 | 36.2 | 15±5 | 1.6 |
| **2d** | 30 | 3 | 613 | 28.0 | 30±10 | 3.1 |
| **2e** | 32 | 4 | 628 | 22.3 | 60±20 | 6.0 |
| **2f** | 34 | 5 | 629 | 17.9 | 80±30 | 7.7 |
| **13a**[14] | 24 | 0 | 471 | 58.5 | 2±1 | 0.31 |
| **1**[12,14] | 26 | 1 | 526 | 45.3 | 6±1 | 0.9 |
| **13c** | 28 | 2 | 570 | 33.6 | 12±4 | 1.6 |
| **13d** | 30 | 3 | 595 | 25.7 | 24±8 | 3.1 |

[a] For each molecule, we give the total number of electrons $N_\pi$ in the two separate conjugated subsystems, the number of C≡C spacers $n$, the longest wavelength absorption maximum $\lambda_{max}$, the corresponding molar extinction coefficient $\varepsilon$, the experimental value of the third-order polarizability $\gamma_{rot}$ (rotational average), and the specific third-order polarizability ($\gamma_S$). The third-order polarizabilities have been measured at a fixed wavelength of 1.5 μm and are increasingly resonantly enhanced for molecules **2d–2f**.

nantly-enhanced $\gamma_{rot}$ value of $(80\pm30)\times10^{-48}\ m^5\,V^{-2}$. For comparison, **1** (DDMEBT) currently used in non-linear optics devices, displays under the same conditions an off-resonant $\gamma_{rot}$ value of $(6\pm1)\times10^{-48}\ m^5\,V^{-2}$.[12]

It is important to note that, as more acetylene moieties are added to the spacers to obtain molecules **2d–f**, the wavelength of maximum absorption shifts towards the red, with the corresponding absorption peak widening towards wavelengths longer than 700 nm. As a consequence, the first two-photon resonance for DFWM approaches the wavelength we used for the measurements (1.5 μm), and the third-order polarizability values obtained for molecules **2d–f** are increasingly enhanced by the closeness to the two-photon absorption condition.

In fact, DFWM experiments performed at longer off-resonant wavelengths confirm that the third-order polarizability values start saturating or even decreasing for the longest oligoyne chains. As a consequence, the specific off-resonant third-order polarizability reaches a maximum for the compounds with two and three triple-bond spacers (**2c**, **d**) and then decreases for the longer molecules. This behavior is consistent with the decrease in the HOMO–LUMO transition dipole moment mentioned above.

## Conclusion

A series of push–pull chromophores **2a–f**, with alkyne spacers of systematically varying length between one anilino donor ring and the TCBD acceptor moiety was synthesized. The effect of this structural change on the spectroscopic and electronic properties of the molecules and, ultimately, on the measured third-order optical nonlinearity was evaluated. The two, independent charge-transfer conjugation pathways in these molecules were comprehensively investigated by means of NMR and UV/Vis spectroscopy, electrochemistry, and theoretical calculations. The branched *N,N*-diisopropylanilino groups and the non-planarity of the donor–acceptor moiety originating from the [2+2] cycloaddition–retroelectrocyclization cascade strongly increased the solubility of these chromophores, thereby allowing for INADEQUATE NMR measurements without $^{13}C$ labeling. These measurements enabled a complete assignment of the carbon skeleton in this series of chromophores and provided unique insight into the electronic properties of these chromophores, such as the π-electron delocalization along the polyyne chain. UV/Vis and electrochemical measurements revealed that the HOMO–LUMO gaps decrease with increasing length of the polyyne chain spacer, while the effect of the spacer length levels off for spacers with more than four acetylene units (saturation). These findings were further corroborated by density functional theory calculations. Also, these conclusions were in complete agreement with the NLO studies, which, in turn, showed a decrease of the specific off-resonant third-order polarizability for chromophores with four- and five-triple-bond spacers (**2e**,**f**). Importantly, the optimal conjugation length, in terms of nonlinear optical response, was provided by the two- and three-triple-bond spacers. Compounds **2d** and **13d** in particular, feature a remarkably high, non-resonantly enhanced third-order optical nonlinearity.

In essence, this investigation provided important insight into the effect of the conjugated spacer length in D–A polyynes, which can be exploited in the future design of suitable CT chromophores with potential applications in optoelectronic devices.

## Experimental Section

General materials and physical characterization data are found in the Supporting Information.

**2D NMR spectra**: INADEQUATE spectra were measured on a Bruker Avance III 600 MHz spectrometer equipped with a 5 mm CPDCH cryogenic probe optimized for carbon sensitivity. Sample concentration in $CDCl_3$ was between 100 and 400 mM. Pulse sequence and phase cycle were taken from reference [53]. The echo delay (1/(4 JCC)) was set to 2.5 ms. Recycle delay (including acquisition time) was between 2 and 3 s. Total experiment time was between 19 and 80 h.

**2,3-Bis[4-(diisopropylamino)phenyl]buta-1,3-diene-1,1,4,4-tetracarbonitrile (2a)**: A solution of **3a** (112 mg, 0.30 mmol) in $CH_2Cl_2$ (3 mL) was treated with TCNE (46 mg, 0.36 mmol) and stirred at 25 °C for 8 h (the reaction color changed from brown-yellow to dark red upon addition of TCNE). Evaporation and column chromatography ($SiO_2$, $CH_2Cl_2$) gave **2a** (135 mg, 90 %) as a black metallic solid. $R_f=0.45$ ($SiO_2$, $CH_2Cl_2$); m.p. 253 °C; $^1H$ NMR (300 MHz, $CDCl_3$, 25 °C): $\delta=1.35$ (d, $J=6.8$ Hz, 24H, H-C(1′)), 4.06 (hept, $J=6.8$ Hz, 4H, (H-C(2′)), 6.82 (d, $J=9.6$ Hz, 4H, H-C(4′)), 7.76 ppm (d, $J=9.5$ Hz, 4H, H-C(5′)); $^{13}C$ NMR (75 MHz, $CDCl_3$, 25 °C): $\delta=20.75$ and 20.83, 48.33 (C(2′)), 73.45 (C(8′)), 113.98 (CN), 114.52 (C(4′)), 115.07 (CN), 118.20 (C(15′)), 132.26 (C(5′)), 153.06 (C(3′)), 164.93 ppm (C(7′)); IR (ATR): $\tilde{\nu}=2975$ (w), 1935 (w), 2215 (m), 1599 (s), 1480 (s), 1445 (s), 1373 (w), 1340 (m), 1309 (s), 1278 (m), 1213 (m), 1187 (m), 1162 (m), 1124 (m), 1016 (w) $cm^{-1}$; UV/Vis ($CH_2Cl_2$): $\lambda_{max}$ ($\varepsilon$) = 260 (13300), 286 (sh, 10400), 413 (sh, 22800), 482 (66800 $M^{-1}cm^{-1}$); HR-MALDI-MS (DCTB): *m/z* (%): 504.2997 (100, $[M]^+$, calcd for $C_{32}H_{36}N_6^+$: 504.2996).

**2-[4-(Diisopropylamino)phenyl]-3-{[4-(diisopropylamino)phenyl]ethynyl}buta-1,3-diene-1,1,4,4-tetracarbonitrile (2b)**: A solution of diyne **3b** (105 mg, 0.26 mmol) in $CH_2Cl_2$ (2 mL) was treated with TCNE (40 mg, 0.31 mmol) and stirred at 25 °C for 8 h (the reaction color changed from brown-yellow to dark red upon addition of TCNE). Evaporation and column chromatography ($SiO_2$, $CH_2Cl_2$) gave **2b** (120 mg, 92 %) as a black metallic solid. $R_f=0.47$ ($SiO_2$, $CH_2Cl_2$); m.p. 204 °C; $^1H$ NMR (300 MHz, $CDCl_3$, 25 °C): $\delta=1.34$ (d, $J=6.9$ Hz, 12H, H-C(1′)), 1.37 (d, $J=6.8$ Hz, 12H, H-C(20′)), 4.01 (hept, $J=6.8$ Hz, 2H, H-C(2′)), 4.07 (hept, $J=6.8$ Hz, 2H, H-C(19′)), 6.78 (d, $J=9.2$ Hz, 2H, H-C(4′)), 6.86 (d, $J=9.5$ Hz, 2H, H-C(17′)), 7.42 (d, $J=9.2$ Hz, 2H, H-C(5′)), 7.79 ppm (d, $J=9.5$ Hz, 2H, H-C(16′)); $^{13}C$ NMR (75 MHz, $CDCl_3$, 25 °C): $\delta=$ 20.78 and 20.86 (C(20′)), 20.78 (C(1′)), 48.03 (C(2′)), 48.39 (C(19′)), 72.61 (C(10′)), 86.87 (C(8′)), 90.55 (C(2)), 104.79 (C(6′)), 111.78 and 112.81 (2 C; C(13′,14′)), 113.69 (C(11′or 12′)), 114.61 (C(17′), 114.77 (C(4′)), 114.92 (C(11′or 12′)), 117.00 (C(15′)), 125.81 (C(1)), 132.21 (C(16′)), 135.73 (C(5′)), 149.95 (C(7′)), 151.79 (C(3′)), 153.26 (C(18′)), 160.78 ppm (C(9′)); IR (ATR): $\tilde{\nu}=2971$ (w), 2937 (w), 2880 (w), 2215 (m), 2119 (s), 1595 (s), 1525 (m), 1484 (s), 1447 (m), 1431 (s), 1382 (m), 1329 (s), 1314 (m), 1293 (m), 1218 (m), 1190 (m), 1166 (w), 1153 (w), 1109 (s), 1011 (m), 988 (w), 827 (m) $cm^{-1}$; UV/Vis ($CH_2Cl_2$): $\lambda_{max}$ ($\varepsilon$) = 284 (17100), 324 (sh, 9600), 441 (sh, 27200), 486 (sh, 35300), 539 (49200 $M^{-1}cm^{-1}$); HR-MALDI-MS (DCTB): *m/z* (%): 528.2997 (100, $[M]^+$, calcd for $C_{34}H_{36}N_6^+$: 528.2996).

**2-[4-(Diisopropylamino)phenyl]-3-{[4-(diisopropylamino)phenyl]buta-1,3-diyn-1-yl}buta-1,3-diene-1,1,4,4-tetracarbonitrile (2c)**: A solution of

triyne **3c** (110 mg, 0.26 mmol) in $CH_2Cl_2$ (16 mL) was treated with TCNE (37 mg, 0.29 mmol) and stirred at 25 °C for 8 h (the reaction color changed from orange to dark blue upon addition of TCNE). Evaporation and column chromatography ($SiO_2$, $CH_2Cl_2$) gave **2c** (119 mg, 83 %) as a black metallic solid. $R_f$ = 0.48 ($SiO_2$, $CH_2Cl_2$); m.p. 133 °C; $^1$H NMR (400 MHz, $CDCl_3$, 25 °C): $\delta$ = 1.32 (d, $J$ = 6.9 Hz, 12H, H-C(1′)), 1.38 (d, $J$ = 6.9 Hz, 12H, H-C(20′)), 3.97 (hept, $J$ = 6.9 Hz, 2H, H-C(2′)), 4.09 (hept, $J$ = 6.9 Hz, 2H, H-C(19′)), 6.75 (d, $J$ = 9.2 Hz, 2H, H-C(4′)), 6.87 (d, $J$ = 9.5 Hz, 2H, H-C(17′)), 7.38 (d, $J$ = 9.0 Hz, 2H, H-C(5′)), 7.75 ppm (d, $J$ = 9.4 Hz, 2H, H-C(16′)); $^{13}$C NMR (101 MHz, $CDCl_3$, 25 °C): $\delta$ = 20.80 (C(20′)), 20.92 (C(1′)), 47.83 (C(2′)), 48.52 (C(19′)), 72.80 (C(10′)), 74.92 (C(2)), 78.25 (C(4)), 92.86 (C(8′)), 104.39 (C(6′)), 104.78 (C(1)), 104.86 (C(3)), 110.93 and 111.81 (2 C; C(13′,14′), 113.64 and 114.64 (2 C; C(11′,12′)), 114.75 (C(17′)), 114.81 (C(4′)), 116.75 (C(15′)), 132.15 (C-(16′)), 135.10 (C(5′)), 150.01 (C(7′)), 150.84 (C(3′)), 153.44 (C(18′)), 159.48 ppm (C(9′)); IR (ATR): $\tilde{\nu}$ = 2971 (m), 2933 (w), 2872 (w), 2214 (m), 2125 (s), 1586 (s), 1509 (s), 1482 (s), 1446 (s), 1383 (m), 1331 (s), 1298 (s), 1218 (m), 1204 (m), 1188 (m), 1153 (s), 1118 (s), 1062 (m), 1017 (m), 821 (m) cm$^{-1}$; UV/Vis ($CH_2Cl_2$): $\lambda_{max}$ ($\varepsilon$) = 352 (19800), 460 (31800), 586 (36200 M$^{-1}$cm$^{-1}$); HR-MALDI-MS (DCTB): $m/z$ (%): 552.2996 (100, $[M]^+$, calcd for $C_{36}H_{36}N_2^+$: 552.2996).

**2-[4-(Diisopropylamino)phenyl]-3-[(4-(diisopropylamino)phenyl)hexa-1,3,5-triyn-1-yl]buta-1,3-diene-1,1,4,4-tetracarbonitrile (2d)**: A solution of tetrayne **3d** (116 mg, 0.26 mmol) in $CH_2Cl_2$ (7 mL) was treated with TCNE (40 mg, 0.310 mmol) and stirred at 25 °C for 8 h (the reaction color changed from dark yellow to dark green upon addition of TCNE). Evaporation and column chromatography ($SiO_2$, $CH_2Cl_2$) gave **2d** (88 mg, 60 %) as a black metallic solid. $R_f$ = 0.53 ($SiO_2$, $CH_2Cl_2$); m.p. 126 °C; $^1$H NMR (400 MHz, $CDCl_3$, 25 °C): $\delta$ = 1.31 (d, $J$ = 6.9 Hz, 12H, H-C(1′)), 1.39 (d, $J$ = 6.9 Hz, 12H, H-C(20′)), 3.95 (d, $J$ = 6.9 Hz, 2H, H-C(2′)), 4.10 (hept, $J$ = 6.9 Hz, 2H, H-C(19′)), 6.74 (d, $J$ = 9.2 Hz, 2H, H-C(4′)), 6.88 (d, $J$ = 9.5 Hz, 2H, H-C(17′)), 7.37 (d, $J$ = 9.0 Hz, 2H, H-C(5′)), 7.71 ppm (d, $J$ = 9.5 Hz, 2H, H-C(16′)); $^{13}$C NMR (101 MHz, $CDCl_3$, 25 °C): $\delta$ = 20.82 (C(20′)), 20.96 (C(1′)), 47.75 (C(C2′)), 48.60 (C-(19′)), 66.24 (C(4)), 72.77 (C(10′)), 72.90 (C(6)), 74.22 (C(2)), 85.63 (C(3)), 93.02 (C(1)), 96.05 (C(8′)), 102.23 (C(5)), 104.03 (C(6′)), 110.49 and 111.34 (2 C; C(13′,14′)), 113.57 and 114.51 (2 C; C(11′,12′)), 114.83 (C(17′), 114.88 (C(4′)), 116.62 (C(15′)), 132.14 (C(16′)), 135.07 (C(5′)), 149.68 (C(7′)), 150.41 (C(3′)), 153.54 (C(18′)), 158.67 ppm (C(9′)); IR (ATR): $\tilde{\nu}$ = 2974 (w), 2935 (w), 2876 (w), 2216 (w), 2174 (w), 2111 (s), 2064 (s), 1590 (s), 1523 (m), 1486 (m), 1448 (m), 1373 (w), 1335 (m), 1300 (m), 1267 (m), 1219 (m), 1190 (m), 1154 (m), 1119 (m), 823 (w) cm$^{-1}$; UV/Vis ($CH_2Cl_2$): $\lambda_{max}$ ($\varepsilon$) = 275 (31100), 342 (23300), 395 (31600), 462 (45000), 613 (28000 M$^{-1}$cm$^{-1}$); HR-MALDI-MS (DCTB): $m/z$ (%): 576.2997 (100, $[M]^+$, calcd for $C_{38}H_{36}N_6^+$: 576.2996).

**2-[4-(Diisopropylamino)phenyl]-3-[(4-(diisopropylamino)phenyl]octa-1,3,5,7-tetrayn-1-yl)buta-1,3-diene-1,1,4,4-tetracarbonitrile (2e)**: A solution of pentayne **3e** (102 mg, 0.22 mmol) in $CH_2Cl_2$ (9 mL) was treated with TCNE (33 mg, 0.26 mmol) and stirred at 25 °C for 8 h (the reaction color changed from red to dark green upon addition of TCNE). Evaporation and column chromatography ($SiO_2$, $CH_2Cl_2$) gave **2e** (72 mg, 56 %) as a black metallic solid. $R_f$ = 0.56 ($SiO_2$, $CH_2Cl_2$); m.p. > 340 °C (decomp); $^1$H NMR (400 MHz, $CDCl_3$, 25 °C): $\delta$ = 1.31 (d, $J$ = 6.9 Hz, 12H, H-C(1′)), 1.39 (d, $J$ = 6.9 Hz, 12H, H-C(20′)), 3.94 (hept, $J$ = 6.9 Hz, 2H, H-C(2′)), 4.10 (hept, $J$ = 6.9 Hz, 2H, H-C(19′)), 6.72 (d, $J$ = 9.2 Hz, 2H, H-C(4′)), 6.88 (d, $J$ = 9.5 Hz, 2H, H-C(17′)), 7.38 (d, $J$ = 9.2 Hz, 2H, H-C(5′)), 7.69 ppm (d, $J$ = 9.5 Hz, 2H, H-C(16′)); $^{13}$C NMR (101 MHz, $CDCl_3$, 25 °C): $\delta$ = 20.85 (C(20′)), 21.01 (C(1′)), 47.73 (C(2′)), 48.66 (C-(19′)), 62.39 (C(6)), 67.15 (C(4)), 70.46 (C(8)), 72.89 (C(10′)), 73.91 (C(2)), 75.25 (C(3)), 84.18(C(5), 87.27(C(1)), 97.56 (C(8′)), 100.70 (C(7)), 104.01 (C(6′)), 110.26 and 111.14 (2 C; C(13′,14′)), 113.53 and 114.43 (2 C; C(11′,12′)), 114.91 (C(17′)), 114.95 (C(4′)), 116.58 (C(15′)), 132.14 (C-(16′)), 135.10 (C(5′)), 149.46 (C(7′)), 150.23 (C(3′)), 153.61 (C(18′)), 158.21 ppm (C(9′)); IR (ATR): $\tilde{\nu}$ = 2973 (w), 2937 (w), 2876 (w), 2215 (w), 2178 (w), 2141 (w), 2057 (s), 1592 (s), 1518 (m), 1486 (m), 1448 (m), 1372 (w), 1335 (m), 1300 (m), 12158 (m), 1197 (m), 1155 (m), 1119 (m), 1018 (w), 821 (w) cm$^{-1}$; UV/Vis ($CH_2Cl_2$): $\lambda_{max}$ ($\varepsilon$) = 298 (sh, 40200), 305 (40900), 324 (sh, 36900), 361 (sh, 28900), 377 (32600), 434 (sh, 47900), 469 (60300), 628 (22300 M$^{-1}$cm$^{-1}$); HR-MALDI-MS (DCTB): $m/z$ (%): 600.2997 (100, $[M]^+$, calcd for $C_{40}H_{36}N_2^+$: 600.2996).

**2-[4-(Diisopropylamino)phenyl]-3-{[4-(diisopropylamino)phenyl]deca-1,3,5,7,9-pentayn-1-yl}buta-1,3-diene-1,1,4,4-tetracarbonitrile (2f)**: A solution of hexayne **3f** (166 mg, 0.33 mmol) in $CH_2Cl_2$ (37 mL) was treated with TCNE (52 mg, 0.40 mmol) and stirred at 25 °C for 8 h (the reaction color changed from red to dark green upon addition of TCNE). Evaporation and column chromatography ($SiO_2$, $CH_2Cl_2$) gave **2f** (105 mg, 50 %) as a black metallic solid. $R_f$ = 0.57 ($SiO_2$, $CH_2Cl_2$); m.p. > 340 °C (decomp); $^1$H NMR (400 MHz, $CDCl_3$, 25 °C): $\delta$ = 1.30 (d, $J$ = 6.9 Hz, 12H, H-C(1′)), 1.39 (d, $J$ = 6.9 Hz, 12H, H-C(20′)), 3.93 (hept, $J$ = 6.9 Hz, 2H, H-C(2′))), 4.10 (hept, $J$ = 6.9 Hz, 2H, H-C(19′)), 6.72 (d, $J$ = 9.2 Hz, 2H, H-C(4′)), 6.87 (d, $J$ = 9.5 Hz, 2H, H-C(17′)), 7.37 (d, $J$ = 9.2 Hz, 2H, H-C(5′)), 7.68 ppm (d, $J$ = 9.5 Hz, 2H, H-C(16′)); $^{13}$C NMR (101 MHz, $CDCl_3$, 25 °C): $\delta$ = 20.76 (C(20′)), 20.93 (C(1′)), 47.73 (C(2′)), 48.69 (C-(19′)), 60.66 (C(8)), 63.96 (C(6)), 67.47 (C(4)), 69.44 (C(10)), 70.28 (C(3)), 72.48 (C(10′)), 73.77 (C(2)), 74.57 (C(5)), 83.03 (C(7)), 84.62 (C(1)), 98.40 (C(8′)), 99.60 (C(9)), 103.77 (C(6′)), 110.13 and 111.02 (2 C; C(13′,14′)), 113.49 and 114.37 (2 C; C(11′,12′)), 114.88 (C(17′)), 114.89 (C(4′)), 116.38 (C(15′)), 132.15 (C(16′)), 135.14 (C(5′)), 149.13 (C(7′)), 150.13 (C(3′)), 153.65 (C(18′)), 157.71 ppm (C(9′)); IR (ATR): $\tilde{\nu}$ = 2972 (m), 2934 (w), 2872 (w), 2215 (m), 2173 (m), 2010 (s), 1587 (s), 1519 (s), 1484 (s), 1445 (s), 1372 (m), 1333 (m), 1297 (s), 1218 (m), 1202 (m), 1188 (m), 1153 (s), 1118 (s), 1085 (m), 1016 (m), 816 (m) cm$^{-1}$; UV/Vis ($CH_2Cl_2$): $\lambda_{max}$ ($\varepsilon$) = 256 (50100), 269 (sh, 47000), 318 (sh, 44100), 333 (49300), 349 (sh, 46100), 409 (43000), 473 (68800), 629 (17900 M$^{-1}$cm$^{-1}$); HR-MALDI-MS (DCTB): $m/z$ (%): 624.2997 (100, $[M]^+$, calcd for $C_{42}H_{36}N_2^+$: 624.2996).

## Acknowledgements

This work was supported by the ERC Advanced Grant No. 246637 ("OPTELOMAC"). B.B. and O.D. acknowledge the receipt of a Kekulé fellowship from the Fonds der Chemischen Industrie. M.B. and I.B. acknowledge support from a Faculty Innovation Grant from Lehigh University.

[1] S. Barlow, S. R. Marder in *Functional Organic Materials* (Eds.: T. J. J. Müller, U. H. F. Bunz), Wiley-VCH, Weinheim, **2007**, pp. 393–437.
[2] R. Gompper, H.-U. Wagner, *Angew. Chem.* **1988**, *100*, 1492–1511; *Angew. Chem. Int. Ed. Engl.* **1988**, *27*, 1437–1455.
[3] Y. Yamashita, M. Tomura, *J. Mater. Chem.* **1998**, *8*, 1933–1944.
[4] H. Meier, *Angew. Chem.* **2005**, *117*, 2536–2561; *Angew. Chem. Int. Ed.* **2005**, *44*, 2482–2506.
[5] B. Albinsson, M. P. Eng, K. Pettersson, M. U. Winters, *Phys. Chem. Chem. Phys.* **2007**, *9*, 5847–5864.
[6] Y. Wu, W. Zhu, *Chem. Soc. Rev.* **2013**, *42*, 2039–2058.
[7] M. Kivala, F. Diederich, *Acc. Chem. Res.* **2009**, *42*, 235–248.
[8] C. Bosshard, R. Spreiter, P. Günter, R. R. Tykwinski, M. Schreiber, F. Diederich, *Adv. Mater.* **1996**, *8*, 231–234.
[9] N. N. P. Moonen, W. C. Pomerantz, R. Gist, C. Boudon, J.-P. Gisselbrecht, T. Kawai, A. Kishioka, M. Gross, M. Irie, F. Diederich, *Chem. Eur. J.* **2005**, *11*, 3325–3341.
[10] J. C. May, J. H. Lim, I. Biaggio, N. N. P. Moonen, T. Michinobu, F. Diederich, *Opt. Lett.* **2005**, *30*, 3057–3059.
[11] G. Jiang, T. Michinobu, W. Yuan, M. Feng, Y. Wen, S. Du, H. Gao, L. Jiang, Y. Song, F. Diederich, D. Zhu, *Adv. Mater.* **2005**, *17*, 2170–2173.
[12] M. T. Beels, M. S. Fleischman, I. Biaggio, B. Breiten, M. Jordan, F. Diederich, *Opt. Mater. Express* **2012**, *2*, 294–303.
[13] S.-i. Kato, F. Diederich, *Chem. Commun.* **2010**, *46*, 1994–2006.
[14] T. Michinobu, J. C. May, J. H. Lim, C. Boudon, J.-P. Gisselbrecht, P. Seiler, M. Gross, I. Biaggio, F. Diederich, *Chem. Commun.* **2005**, 737–739.

  

[15] T. Michinobu, C. Boudon, J.-P. Gisselbrecht, P. Seiler, B. Frank, N. N. P. Moonen, M. Gross, F. Diederich, *Chem. Eur. J.* **2006**, *12*, 1889–1905.
[16] S.-i. Kato, M. T. R. Beels, P. La Porta, W. B. Schweizer, C. Boudon, J.-P. Gisselbrecht, I. Biaggio, F. Diederich, *Angew. Chem.* **2010**, *122*, 6343–6347; *Angew. Chem. Int. Ed.* **2010**, *49*, 6207–6211.
[17] M. Chiu, B. Jaun, M. T. R. Beels, I. Biaggio, J.-P. Gisselbrecht, C. Boudon, W. B. Schweizer, M. Kivala, F. Diederich, *Org. Lett.* **2012**, *14*, 54–57.
[18] C. Koos, P. Vorreau, T. Vallaitis, P. Dumon, W. Bogaerts, R. Baets, B. Esembeson, I. Biaggio, T. Michinobu, W. Freude, J. Leuthold, *Nat. Photonics* **2009**, *3*, 216–219.
[19] B. Esembeson, M. L. Scimeca, T. Michinobu, F. Diederich, I. Biaggio, *Adv. Mater.* **2008**, *20*, 4584–4587.
[20] C. Dehu, F. Meyers, J. L. Brédas, *J. Am. Chem. Soc.* **1993**, *115*, 6198–6206.
[21] A. E. Stiegman, E. Graham, K. J. Perry, L. R. Khundkar, L.-T. Cheng, J. W. Perry, *J. Am. Chem. Soc.* **1991**, *113*, 7658–7666.
[22] E. M. Graham, V. M. Miskowski, J. W. Perry, D. R. Coulter, A. E. Stiegman, W. P. Schaefer, R. E. Marsh, *J. Am. Chem. Soc.* **1989**, *111*, 8771–8779.
[23] A. E. Stiegman, V. M. Miskowski, J. W. Perry, D. R. Coulter, *J. Am. Chem. Soc.* **1987**, *109*, 5884–5886.
[24] N. Matsuzawa, D. A. Dixon, *Int. J. Quantum Chem.* **1992**, *44*, 497–515.
[25] J. O. Morley, *Int. J. Quantum Chem.* **1993**, *46*, 19–26.
[26] M. Jain, J. Chandrasekhar, *J. Phys. Chem.* **1993**, *97*, 4044–4049.
[27] J. Y. Lee, S. B. Suh, K. S. Kim, *J. Chem. Phys.* **2000**, *112*, 344–348.
[28] B. Witulski, T. Schweikert, D. Schollmeyer, N. A. Nemkovich, *Chem. Commun.* **2010**, *46*, 2953–2955.
[29] J. A. Armstrong, N. Bloembergen, J. Ducuing, P. S. Pershan, *Phys. Rev.* **1962**, *127*, 1918–1939.
[30] A. D. Slepkov, F. A. Hegmann, S. Eisler, E. Elliot, R. R. Tykwinski, *J. Chem. Phys.* **2004**, *120*, 6807–6810.
[31] T. Luu, E. Elliot, A. D. Slepkov, S. Eisler, R. McDonald, F. A. Hegmann, R. R. Tykwinski, *Org. Lett.* **2005**, *7*, 51–54.
[32] S. Eisler, A. D. Slepkov, E. Elliot, T. Luu, R. McDonald, F. A. Hegmann, R. R. Tykwinski, *J. Am. Chem. Soc.* **2005**, *127*, 2666–2676.
[33] R. R. Tykwinski, U. Gubler, R. E. Martin, F. Diederich, C. Bosshard, P. Günter, *J. Phys. Chem. B* **1998**, *102*, 4451–4465.
[34] U. Gubler, R. Spreiter, C. Bosshard, P. Günter, R. R. Tykwinski, F. Diederich, *Appl. Phys. Lett.* **1998**, *73*, 2396–2398.
[35] N. N. P. Moonen, R. Gist, C. Boudon, J.-P. Gisselbrecht, P. Seiler, T. Kawai, A. Kishioka, M. Gross, M. Irie, F. Diederich, *Org. Biomol. Chem.* **2003**, *1*, 2032–2034.
[36] H. Meier, J. Gerold, H. Kolshorn, B. Mühling, *Chem. Eur. J.* **2004**, *10*, 360–370.
[37] N. N. P. Moonen, F. Diederich, *Org. Biomol. Chem.* **2004**, *2*, 2263–2266.
[38] F. Bureš, W. B. Schweizer, J. C. May, C. Boudon, J.-P. Gisselbrecht, M. Gross, I. Biaggio, F. Diederich, *Chem. Eur. J.* **2007**, *13*, 5378–5387.
[39] B. B. Frank, P. R. Laporta, B. Breiten, M. C. Kuzyk, P. D. Jarowski, W. B. Schweizer, P. Seiler, I. Biaggio, C. Boudon, J.-P. Gisselbrecht, F. Diederich, *Eur. J. Org. Chem.* **2011**, 4307–4317.
[40] B. B. Frank, M. Kivala, B. C. Blanco, B. Breiten, W. B. Schweizer, P. R. Laporta, I. Biaggio, E. Jahnke, R. R. Tykwinski, C. Boudon, J.-P. Gisselbrecht, F. Diederich, *Eur. J. Org. Chem.* **2010**, 2487–2503.
[41] For reviews of this chemistry, see references [7] and [1].
[42] M. Kivala, C. Boudon, J.-P. Gisselbrecht, P. Seiler, M. Gross, F. Diederich, *Angew. Chem.* **2007**, *119*, 6473–6477; *Angew. Chem. Int. Ed.* **2007**, *46*, 6357–6360.
[43] B. Breiten, Y.-L. Wu, P. D. Jarowski, J.-P. Gisselbrecht, C. Boudon, M. Griesser, C. Onitsch, G. Gescheidt, W. B. Schweizer, N. Langer, C. Lennartz, F. Diederich, *Chem. Sci.* **2011**, *2*, 88–93.
[44] S. Eisler, N. Chahal, R. McDonald, R. R. Tykwinski, *Chem. Eur. J.* **2003**, *9*, 2542–2550.
[45] T. Luu, Y. Morisaki, N. Cunningham, R. R. Tykwinski, *J. Org. Chem.* **2007**, *72*, 9622–9629.
[46] E. Jahnke, R. R. Tykwinski, *Chem. Commun.* **2010**, *46*, 3235–3249.
[47] W. A. Chalifoux, R. R. Tykwinski, *Chem. Rec.* **2006**, *6*, 169–182.
[48] A. Auffrant, F. Diederich, C. Boudon, J.-P. Gisselbrecht, M. Gross, *Helv. Chim. Acta* **2004**, *87*, 3085–3105.
[49] T. E. O. Screen, K. B. Lawton, G. S. Wilson, N. Dolney, R. Ispasoiu, T. Goodson, S. J. Martin, D. D. C. Bradley, H. L. Anderson, *J. Mater. Chem.* **2001**, *11*, 312–320.
[50] Y.-Q. Fang, O. Lifchits, M. Lautens, *Synlett* **2008**, 413–417.
[51] A. Bax, R. Freeman, S. P. Kempsell, *J. Am. Chem. Soc.* **1980**, *102*, 4849–4851.
[52] a) D. Uhrín, Recent developments in liquid-state INADEQUATE studies, in *Annual Reports on NMR Spectroscopy, Vol. 70* (Ed.: G. A. Webb), Elsevier, London, **2010**, pp. 1–34; b) J. Buddrus, J. Lambert, *Magn. Reson. Chem.* **2002**, *40*, 3–23.
[53] A. D. Bain, D. W. Hughes, C. K. Anand, Z. Nie, V. J. Robertson, *Magn. Reson. Chem.* **2010**, *48*, 630–641.
[54] F. Tancini, Y.-L. Wu, W. B. Schweizer, J.-P. Gisselbrecht, C. Boudon, P. D. Jarowski, M. T. Beels, I. Biaggio, F. Diederich, *Eur. J. Org. Chem.* **2012**, 2756–2765.
[55] R. R. Tykwinski, T. Luu, *Synthesis* **2012**, 1915–1922.
[56] F. L. Hirshfeld, *Theor. Chim. Acta* **1977**, *44*, 129–138.
[57] Gaussian 09, Revision A.01, M. J. Frisch, G. W. Trucks, H. B. Schlegel, G. E. Scuseria, M. A. Robb, J. R. Cheeseman, G. Scalmani, V. Barone, B. Mennucci, G. A. Petersson, H. Nakatsuji, M. Caricato, X. Li, H. P. Hratchian, A. F. Izmaylov, J. Bloino, G. Zheng, J. L. Sonnenberg, M. Hada, M. Ehara, K. Toyota, R. Fukuda, J. Hasegawa, M. Ishida, T. Nakajima, Y. Honda, O. Kitao, H. Nakai, T. Vreven, J. A. Montgomery, Jr., J. E. Peralta, F. Ogliaro, M. Bearpark, J. J. Heyd, E. Brothers, K. N. Kudin, V. N. Staroverov, R. Kobayashi, J. Normand, K. Raghavachari, A. Rendell, J. C. Burant, S. S. Iyengar, J. Tomasi, M. Cossi, N. Rega, J. M. Millam, M. Klene, J. E. Knox, J. B. Cross, V. Bakken, C. Adamo, J. Jaramillo, R. Gomperts, R. E. Stratmann, O. Yazyev, A. J. Austin, R. Cammi, C. Pomelli, J. W. Ochterski, R. L. Martin, K. Morokuma, V. G. Zakrzewski, G. A. Voth, P. Salvador, J. J. Dannenberg, S. Dapprich, A. D. Daniels, Ö. Farkas, J. B. Foresman, J. V. Ortiz, J. Cioslowski, D. J. Fox, Gaussian, Inc. Wallingford CT, **2009**.
[58] F. Bohlmann, M. Brehm, *Chem. Ber.* **1979**, *112*, 1071–1073.
[59] C. J. Jödicke, H. P. Lüthi, *J. Am. Chem. Soc.* **2003**, *125*, 252–264.
[60] C. J. Jödicke, H. P. Lüthi, *J. Chem. Phys.* **2002**, *117*, 4146–4156.
[61] D. Jacquemin, V. Wathelet, E. A. Perpète, C. Adamo, *J. Chem. Theory Comput.* **2009**, *5*, 2420–2435.
[62] A saturation of the linear optical properties at significantly shorter chain-length had previously been observed in α,ω-(*N*,*N*-dimethylanilino)- or α,ω-(4-nitrophenyl)-substituted poly(triacetylene)oligomers as compared to silyl-end-capped derivatives; see: a) R. E. Martin, U. Gubler, C. Boudon, C. Bosshard, J.-P. Gisselbrecht, P. Günter, M. Gross, F. Diederich, *Chem. Eur. J.* **2000**, *6*, 4400–4412; b) R. E. Martin, T. Mäder, F. Diederich, *Angew. Chem.* **1999**, *111*, 834–838; *Angew. Chem. Int. Ed.* **1999**, *38*, 817–821.

Received: April 29, 2013
Published online: ■■ ■■, 0000

  